

Bifunctional Transition Metal Hydroxysulfides: Room-Temperature Sulfurization and Their Applications in Zn–Air Batteries

Hao-Fan Wang, Cheng Tang, Bin Wang, Bo-Quan Li, and Qiang Zhang*

Bifunctional electrocatalysis for oxygen evolution reaction (OER) and oxygen reduction reaction (ORR) constitutes the bottleneck of various sustainable energy devices and systems like rechargeable metal–air batteries. Emerging catalyst materials are strongly requested toward superior electrocatalytic activities and practical applications. In this study, transition metal hydroxysulfides are presented as bifunctional OER/ORR electrocatalysts for Zn–air batteries. By simply immersing Co-based hydroxide precursor into solution with high-concentration S^{2-} , transition metal hydroxides convert to hydroxysulfides with excellent morphology preservation at room temperature. The as-obtained Co-based metal hydroxysulfides are with high intrinsic reactivity and electrical conductivity. The electron structure of the active sites is adjusted by anion modulation. The potential for 10 mA cm^{-2} OER current density is 1.588 V versus reversible hydrogen electrode (RHE), and the ORR half-wave potential is 0.721 V versus RHE, with a potential gap of 0.867 V for bifunctional oxygen electrocatalysis. The $Co_3FeS_{1.5}(OH)_6$ hydroxysulfides are employed in the air electrode for a rechargeable Zn–air battery with a small overpotential of 0.86 V at 20.0 mA cm^{-2} , a high specific capacity of 898 mAh g^{-1} , and a long cycling life, which is much better than Pt and Ir-based electrocatalyst in Zn–air batteries.

As the demand for energy continues to rise, the use of emerging energy materials to harvest sustainable energy sources is attracting increasing attention. Transition metal sulfides, oxides, and hydroxides have demonstrated outstanding performance in electrochemical energy storage and conversion.^[1,2] Among various energy materials, bifunctional electrocatalysts for the oxygen evolution reaction (OER) and oxygen reduction reaction (ORR) on the air cathodes are the bottlenecks in metal–air batteries and reversible fuel cells. This is attributed to the sluggish kinetics^[3] and different active sites of the OER and ORR in a


working cell.^[4] Co- and Mn-based oxides and hydroxides were first investigated as nonprecious metal bifunctional electrocatalysts for the OER and ORR and exhibited excellent intrinsic reactivities.^[5] However, the need still remains to achieve bifunctional electrocatalysts as replacements for precious metal materials in bulk applications for energy conversion devices based on oxygen electrocatalysis.^[6,7]

Transition metal chalcogenides are promising due to their high intrinsic reactivities, tunable reactivities, excellent stabilities, and superb electrical conductivities for the OER/ORR, and compounds with multiple anions (e.g., O^{2-} incorporated sulfides) are attracting much attention.^[8–10] In most cases of synthesizing sulfur-containing materials, high-temperature material processing is requested during hydrothermal and/or chemical vapor deposition with hydroxides, oxides, metals, or alloys as precursors.^[2,11–13] Some environmentally unfriendly organic sulfides (such as thiourea and thioacetamide) are employed as sulfurizing

reagents, and the products tend to agglomerate into larger particles than the precursor.^[12,14] Therefore, obtaining sulfurous metal compound-based electrocatalysts with high intrinsic OER/ORR reactivities through a mild and facile approach is strongly considered.

In this contribution, we propose a unique hydroxysulfide electrocatalyst with the integration of hydroxides and sulfides at an atomic level for bifunctional electrocatalysis in Zn–air batteries. The hydroxysulfides are synthesized using a green room-temperature sulfurization strategy by simply immersing metal hydroxide precursors in a solution with a high concentration of S^{2-} , and the S^{2-} continuously replaces the OH^- in the solid phase according to the solubility equilibrium. Ultimately, metal hydroxysulfides converted from hydroxides are therefore achieved. The hydroxysulfides can precisely replicate the morphologies of the hydroxide precursors, which can avoid the strong agglomeration of sulfides seen previously in high-temperature materials processing. Furthermore, a CoFe-based hydroxysulfide electrocatalyst is obtained to render a high bifunctional activity superior to that of precious metal catalysts (e.g., Ir/C and Pt/C), with the potential to achieve a 10.0 mA cm^{-2} OER current density (E_{10}) of 1.588 V and an ORR

H.-F. Wang, C. Tang, Dr. B. Wang, B.-Q. Li, Prof. Q. Zhang
Beijing Key Laboratory of Green Chemical Reaction
Engineering and Technology
Department of Chemical Engineering
Tsinghua University
Beijing 100084, China
E-mail: zhang-qiang@mails.tsinghua.edu.cn

 The ORCID identification number(s) for the author(s) of this article can be found under <https://doi.org/10.1002/adma.201702327>.

DOI: 10.1002/adma.201702327

half-wave potential ($E_{1/2}$) of 0.721 V (vs reversible hydrogen electrode (RHE)). The hydroxysulfide catalyst also serves as a superb air cathode catalyst in high-performance rechargeable Zn–air batteries.

Among various transition metal-based electrocatalysts, Co-based materials are some of the most promising transition metal bifunctional electrocatalysts for the OER and ORR.^[15] With the cooperation of Ni or Fe metals, the catalytic performance of the OER/ORR in CoNi- or CoFe-based electrocatalysts can be even better.^[16,17] To demonstrate the concept of the room-temperature sulfurization process, the monometallic Co(II) hydroxide is chosen as a model system in this contribution.

The solubility product (K_{sp}) of Co(OH)_2 at 25 °C is 1.6×10^{-15} , and the K_{sp} of CoS is 4×10^{-21} (the dissolution of CoS follows this equation: $\text{CoS(s)} + \text{H}_2\text{O(l)} \rightleftharpoons \text{Co}^{2+}(\text{aq}) + \text{HS}^-(\text{aq}) + \text{OH}^-(\text{aq})$). In Na_2S solution, the S^{2-} can be approximate to be completely hydrolyzed to HS^- and OH^- . Therefore, to immerse Co(II) hydroxide into an Na_2S solution (2.0 M), the concentration of OH^- required to reach the solubility equilibrium is 8×10^5 M (see details in the Supporting Information), which is not satisfied in an actual system. Consequently, the transition hydroxides continuously convert to sulfides driven by the thermodynamic equilibrium. This method is applicable to many other transition metal hydroxides by matching the solubility product of their hydroxides and sulfides.

To experimentally verify the feasibility of the room-temperature sulfurization method, CoAl layered double hydroxide (LDH) (denoted as CoAl-OH) was then investigated. In addition to the Co as the active species in the electrocatalysis, the CoAl-OH is advantageous to the formation of a regular hexagonal platelet-shaped structure, thereby facilitating the structural and component characterization. The CoAl-OH was synthesized through a coprecipitation method. Then, the CoAl-OH underwent a room-temperature sulfurization process, in which the hydroxides were immersed in a 2.0 M Na_2S solution at room temperature (≈ 25 °C) for 24 h. While being mixed with the Na_2S solution, the pink CoAl-OH powder immediately turned black, indicating the rapid generation of sulfides on the surface, and the immersion time was set to 24 h for a higher conversion rate.

The facile conversion of CoAl hydroxides to hydroxysulfides is confirmed by X-ray photoelectron spectrum (XPS) and X-ray diffraction (XRD) analysis. The CoAl hydroxysulfide is termed $\text{Co}_5\text{AlS}_{1.5}(\text{OH})_{10}$ according to the XPS analysis (Figure 1a and Figure S1, Supporting Information). After the room-temperature immersing treatment, the S atomic content increased from nearly zero to 12.1% at the surface, and the O content decreased from 57.0% to 42.3% (Table S1, Supporting Information), demonstrating that the OH^- in the solid phase was partly replaced by S^{2-} . The XRD pattern (Figure 1b) of CoAl-OH is consistent with CoAl LDH (JCPDS No. 51-0045). No obvious peak is observed in the XRD pattern of $\text{Co}_5\text{AlS}_{1.5}(\text{OH})_{10}$ electrocatalyst, indicating an amorphous structure after the sulfurization. The cooperation of the cobalt hydroxides and sulfides in the hydroxysulfide induces the lack of long-range crystalline order and, therefore, the amorphous hydroxysulfide structure,^[18] and the amorphous structure is beneficial to the enhanced bifunctional OER/ORR performance.^[19]

The structure of CoAl-OH and $\text{Co}_5\text{AlS}_{1.5}(\text{OH})_{10}$ was further investigated by the scanning electron microscopy (SEM).

As shown in Figure 1c and Figure S2 (Supporting Information), the SEM image confirms the hexagonal structure of the CoAl-OH nanosheets, and the lateral size is ≈ 1 μm . This uniform morphology can facilitate the observation of the structure evolution during room-temperature sulfurization. The transmission electron microscopy (TEM) image of the CoAl-OH (Figure 1d) exhibits the smooth, straight edge of the hydroxide nanosheets. This regulated structure and the selected area electron diffraction (SAED) pattern (Figure 1e) further verify the crystalline state of CoAl-OH. The energy-dispersive X-ray spectrometry (EDS) mapping analysis of O and S (Figure S3, Supporting Information) confirms the absence of S in CoAl-OH.

Figure 1f and Figure S4 (Supporting Information) present the SEM images of $\text{Co}_5\text{AlS}_{1.5}(\text{OH})_{10}$. The platelet-shaped structure is well preserved after the room-temperature sulfurization, while the smooth surface of the nanosheets becomes wrinkled and the straight edge becomes uneven. This structure is also observed by TEM (Figure 1g). The SAED pattern (Figure 1h) shows only broad rings. The EDS mapping image in Figure S5 (Supporting Information) confirms a homogeneous distribution of sulfur atoms in the as-prepared $\text{Co}_5\text{AlS}_{1.5}(\text{OH})_{10}$. These phenomena confirm that the surface OH^- dissolved in the solution and the S^{2-} precipitated out and that the newly formed hydroxysulfides have poor crystallinity. From the above characterizations, it is clear that the hydroxides can easily convert to hydroxysulfides while maintaining the original particle size and shape through the facile immersion treatment.

The electrocatalytic performances of $\text{Co}_5\text{AlS}_{1.5}(\text{OH})_{10}$ and CoAl-OH were probed in 0.10 M KOH electrolyte (Figure 1i,j). $\text{Co}_5\text{AlS}_{1.5}(\text{OH})_{10}$ hydroxysulfide exhibits superior activity to CoAl-OH hydroxide in both OER and ORR catalysis. From the OER linear sweep voltammetry (LSV) plots (Figure 1i), the potential to achieve a 10.0 mA cm^{-2} current density (E_{10}) of $\text{Co}_5\text{AlS}_{1.5}(\text{OH})_{10}$ is 1.644 V, much lower than that of CoAl-OH (1.820 V). Regarding the ORR (Figure 1j), $\text{Co}_5\text{AlS}_{1.5}(\text{OH})_{10}$ exhibits a higher current density and larger electron transfer number than the CoAl-OH electrocatalyst.

An electrochemical impedance spectroscopy test was carried out to elucidate the origin of the activity enhancement on the hydroxysulfide electrocatalyst (Figure S6a, Supporting Information). The charge transfer resistance (R_{ct}) in the equivalent circuit (Figure S6b, Supporting Information) is related to the resistance of the chemical reaction reflecting the intrinsic activity of the electrocatalyst; the resistance of the catalyst layer (R_f) represents the electrical conductivity of the electrocatalyst. The fitting results reveal that the R_{ct} and R_f for $\text{Co}_5\text{AlS}_{1.5}(\text{OH})_{10}$ hydroxysulfides are 17.1 and 33.5 Ω , respectively. Both are much smaller than those of the CoAl-OH ($R_{ct} = 92.5$ Ω , $R_f = 86.3$ Ω) electrocatalyst. The intrinsic activity and electrical conductivity are both enhanced after the sulfurization treatment, which leads to a better electrocatalytic OER/ORR activity.^[13] Based on the above analyses, the room-temperature immersion sulfurization strategy is confirmed to be facile and very effective in both converting hydroxides to hydroxysulfides with the morphology preservation and enhancing the OER/ORR reactivity.

After both the theoretical and experimental proof of the proposed room-temperature immersing sulfurization concept, a practical electrocatalyst system was applied to generalize

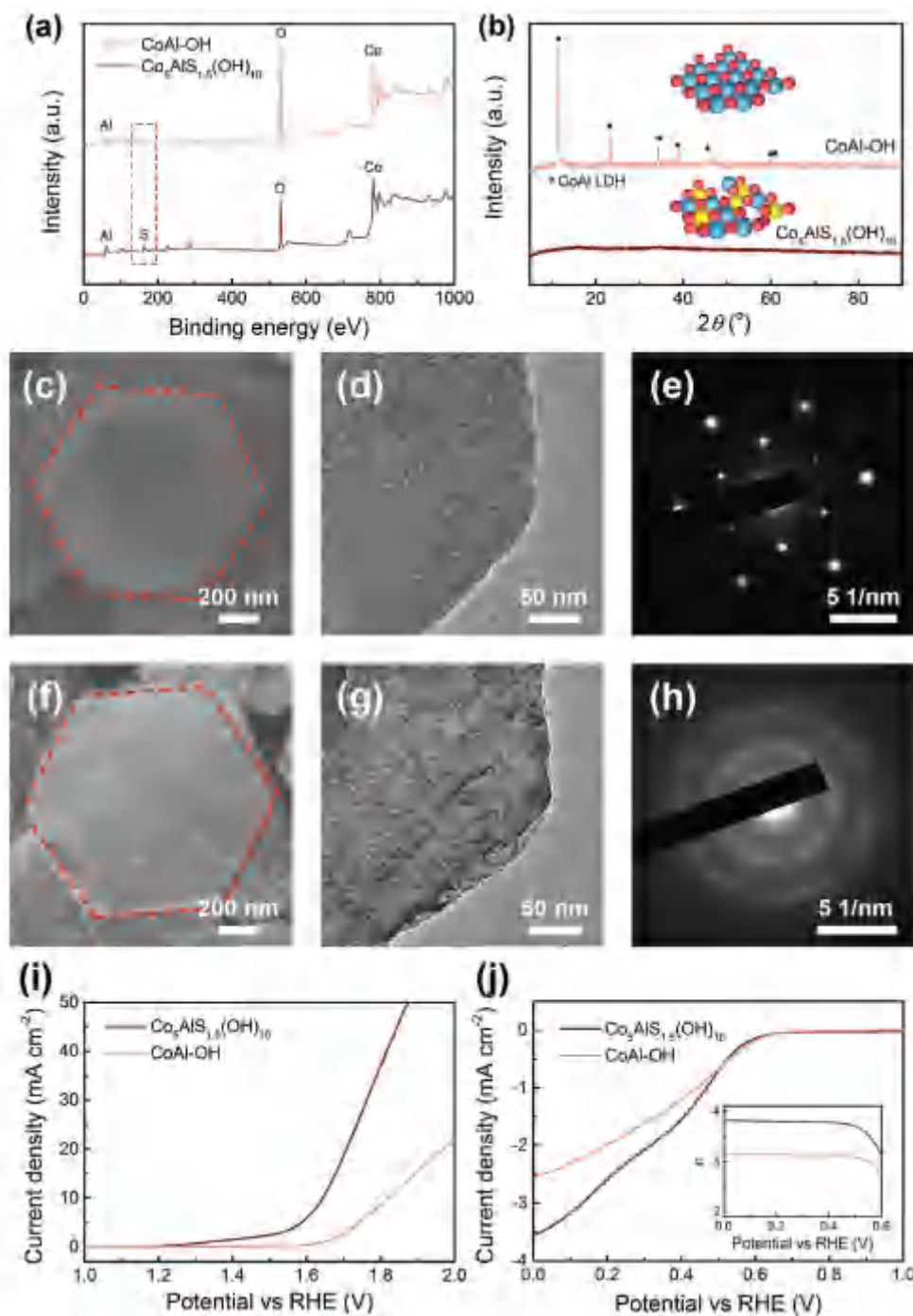


Figure 1. The structural characterization and electrocatalytic activity of the CoAl-OH and $\text{Co}_5\text{AlS}_{1.5}(\text{OH})_{10}$ samples. a) XPS spectra of CoAl-OH and $\text{Co}_5\text{AlS}_{1.5}(\text{OH})_{10}$. b) XRD spectra of CoAl-OH and $\text{Co}_5\text{AlS}_{1.5}(\text{OH})_{10}$. Inset: Schematic of the metal hydroxides and metal hydroxysulfides (red ball: metal ion; blue ball: OH^- ; yellow ball: S^{2-}). c–e) SEM image, TEM image, and SAED pattern of CoAl-OH. f–h) SEM image, TEM image, and SAED pattern of $\text{Co}_5\text{AlS}_{1.5}(\text{OH})_{10}$. i) OER LSV plots of CoAl-OH and $\text{Co}_5\text{AlS}_{1.5}(\text{OH})_{10}$. j) ORR LSV plots of CoAl-OH and $\text{Co}_5\text{AlS}_{1.5}(\text{OH})_{10}$, inset: ORR electron transfer number. The electrochemical tests were carried out in an O_2 -saturated 0.10 M KOH electrolyte at a scan rate of 10.0 mV s^{-1} and a rotating speed of 1600 rpm.

the hydroxysulfide formation through the room-temperature sulfurization strategy. Graphene-supported CoFe hydroxide nanoparticles (CoFe-OH) were chosen herein. In this case, the incorporation of Fe is believed to enhance the activity of

Co-based materials; the graphene can increase the electrical conductivity and the exposure of active sites on hydroxysulfides to the electrolyte, which is expected to result in superb ORR/OER electrocatalysis.

CoFe-OH was fabricated by the hydrothermal growth of hydroxides on nitrogen-doped graphene. The Co:Fe molar ratio was 3:1. With the N sites on graphene as the nucleation sites, the hydroxides can be well dispersed onto the 3D N-doped graphene framework (Figure 2a). The particle size of CoFe-OH is limited to only 20 nm due to the space confinement of the 3D graphene scaffolds (Figure 2d). The CoFe-OH was immersed in a 2.0 M Na₂S solution at room temperature for 24 h during the room-temperature sulfurization, and the as-obtained hydroxy-sulfides were named Co₃FeS_{1.5}(OH)₆.

The SEM and TEM images of the Co₃FeS_{1.5}(OH)₆ are presented in Figure 2b,e, respectively. Compared with CoFe-OH, the S atomic content increased from zero to 10.9%, as revealed by the XPS analysis, and the morphology of the Co₃FeS_{1.5}(OH)₆

was almost unaltered. In contrast, the traditional high-temperature hydrothermally converted CoFe hydroxysulfide from CoFe-OH (denoted as CoFeS_{1.6}(OH)_{1.8}-HT) exhibited much larger particle sizes up to 200 nm (Figure 2c,f). The TEM images of a larger region (Figure S7, Supporting Information) further confirm the structure of the CoFe hydroxides and hydroxysulfides.

The elemental compositions of CoFe-OH and the sulfurized electrocatalysts calculated based on XPS data are shown in Figure 2g and Table S2 (Supporting Information). The relative content of the elements presented in the figure is relative to the content of Fe. In addition to the morphology features, the Co₃FeS_{1.5}(OH)₆ preserved the Co:Fe ratio of CoFe-OH at ≈3:1. In contrast, the Co:Fe ratio in CoFeS_{1.6}(OH)_{1.8}-HT decreased to

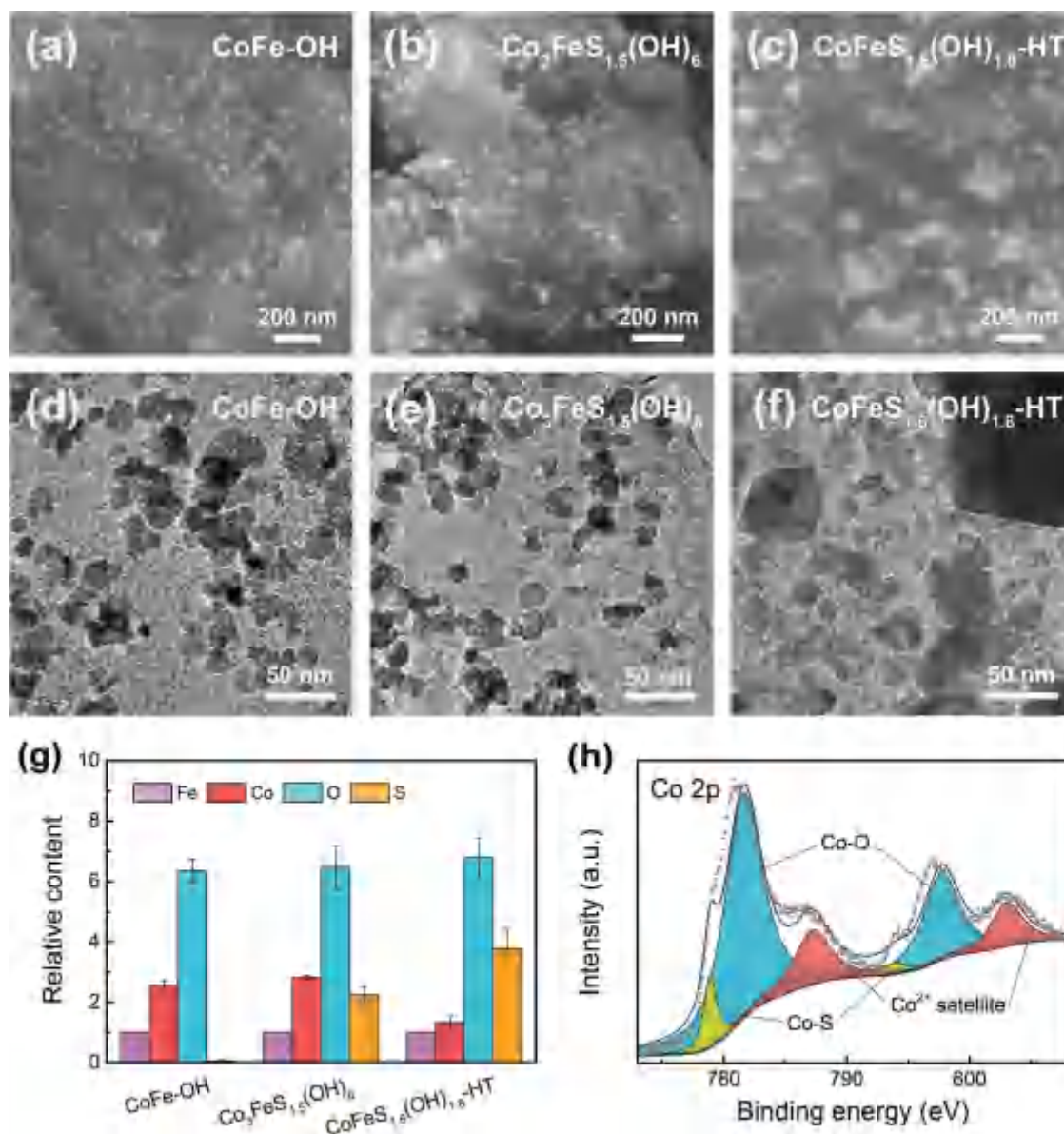


Figure 2. Structural characterizations of the hydroxide precursor CoFe-OH, room-temperature synthesized Co₃FeS_{1.5}(OH)₆, and high-temperature hydrothermally synthesized CoFeS_{1.6}(OH)_{1.8}-HT: a–c) SEM images and d–f) TEM images. g) The contents of Fe, Co, O, and S relative to the Fe content in each material, calculated based on XPS analysis. h) XPS Co 2p spectrum of Co₃FeS_{1.5}(OH)₆.

≈1:1, which is attributed to complex reactions at a high sulfuration temperature during the hydrothermal treatment.

The high resolution XPS Co 2p spectrum of $\text{Co}_3\text{FeS}_{1.5}(\text{OH})_6$ is shown in Figure 2h. The two peaks at ≈778.9 and 793.9 eV can be identified as the peaks of the Co–S bond. The peaks at 781.6 and 797.7 eV are attributed to the Co–O bond. The satellite peaks at 787.2 and 803.0 eV belong to the Co^{2+} ions.^[9] The Fe–S bond and Fe–O bond can also be identified in the Fe 2p spectrum of $\text{Co}_3\text{FeS}_{1.5}(\text{OH})_6$ (Figure S8, Supporting Information).^[8] The XPS results confirm the coexistence of metal–S and metal–O bonds in both the CoFe hydroxysulfides converted at room temperature and the high-temperature-synthesized material (Figure S9, Supporting Information). The formula of the CoFe hydroxysulfides is also determined by the XPS analysis (see details in the Supporting Information).

The OER and ORR performances of the CoFe hydroxysulfides, as well as two precious metal catalysts Ir/C and Pt/C, are shown in Figure 3. The OER LSV and Tafel plots are presented in Figure 3a,b, respectively. The room-temperature synthesized $\text{Co}_3\text{FeS}_{1.5}(\text{OH})_6$ exhibits a higher current density than the $\text{CoFeS}_{1.6}(\text{OH})_{1.8}$ -HT and the precious metal catalysts. The Tafel slope of $\text{Co}_3\text{FeS}_{1.5}(\text{OH})_6$, $\text{CoFeS}_{1.6}(\text{OH})_{1.8}$ -HT, and Ir/C are 79, 82, and 74 mV dec⁻¹, respectively. The similar Tafel slope of the hydroxysulfides to the commercial Ir/C catalyst indicates a high intrinsic activity. The ORR LSV plots

(Figure 3c) reveal that $\text{Co}_3\text{FeS}_{1.5}(\text{OH})_6$ also has superior activity to $\text{CoFeS}_{1.6}(\text{OH})_{1.8}$ -HT for the ORR electrocatalysis, and the Tafel slopes of hydroxysulfides are even lower than for commercial Pt/C (Figure 3d).

The potential to achieve a 10.0 mA cm⁻² OER current density (E_{10}) and the ORR half-wave potential ($E_{1/2}$) are widely used to evaluate the OER and ORR reactivity, respectively. The difference between them (ΔE) can quantitatively describe the bifunctional activity. The ΔE of $\text{Co}_3\text{FeS}_{1.5}(\text{OH})_6$ is 0.867 V ($E_{10} = 1.588$ V, $E_{1/2} = 0.721$ V), which is smaller than for $\text{CoFeS}_{1.6}(\text{OH})_{1.8}$ -HT (0.922 V), verifying the superiority of the room-temperature sulfuration strategy. Moreover, the ΔE of $\text{Co}_3\text{FeS}_{1.5}(\text{OH})_6$ is even smaller than those for commercial precious metal catalysts Ir/C (0.923 V) and Pt/C (0.970 V).

The origin of the outstanding bifunctional activity of $\text{Co}_3\text{FeS}_{1.5}(\text{OH})_6$ is elucidated from the well-dispersed nanostructures and the high intrinsic reactivity. The structural advantages include nanosized catalyst particles, an amorphous surface, and numerous electron pathways in the graphene-supported CoFe hydroxysulfides, thus providing the full exposure of active sites and benefiting electron transfer during the oxygen redox reaction.

The intrinsic activity is enhanced by both cation and anion modulation. The incorporation of Fe species can lower the oxidation state of Co and weaken the Co–O bonds during the oxygen

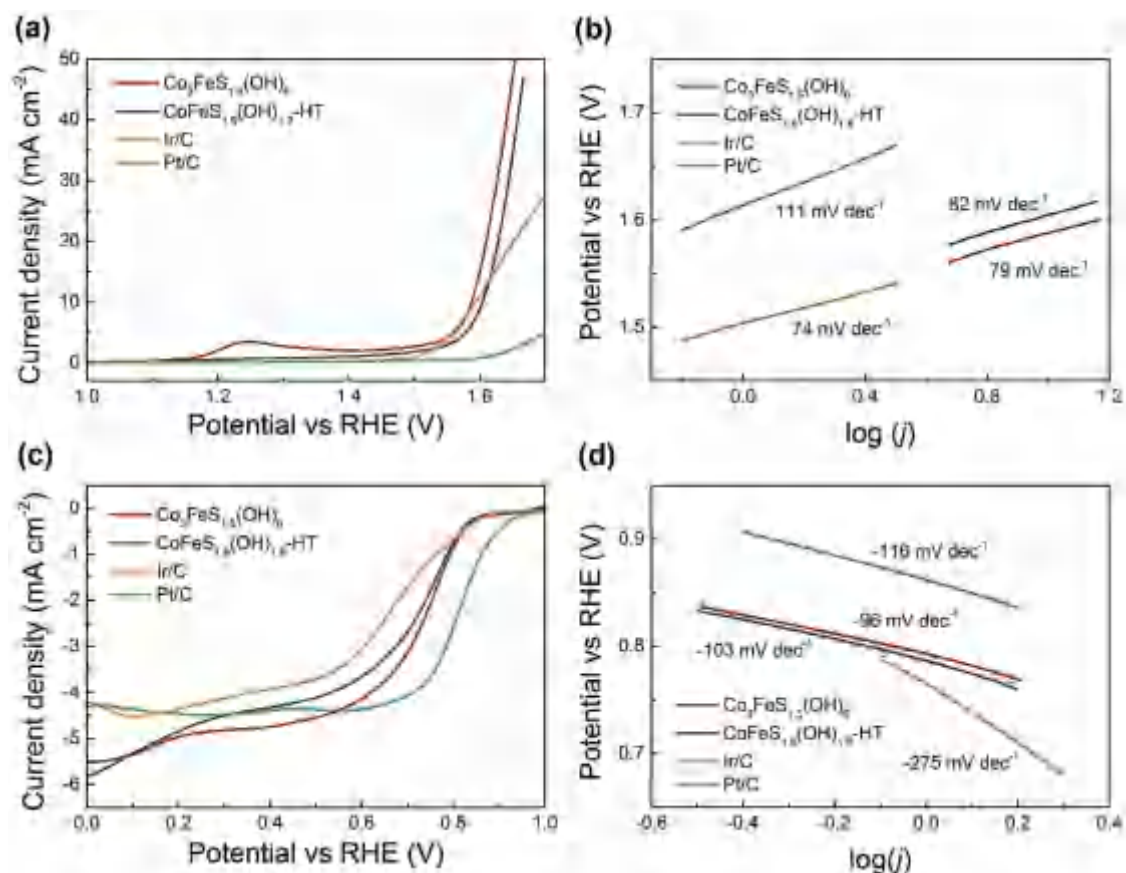


Figure 3. The OER and ORR performance of $\text{Co}_3\text{FeS}_{1.5}(\text{OH})_6$, $\text{CoFeS}_{1.6}(\text{OH})_{1.8}$ -HT, and precious metal catalysts. a) OER LSV plots. b) OER Tafel plots. c) ORR LSV plots. d) ORR Tafel plots. The electrochemical tests were performed in an O_2 -saturated 0.10 M KOH electrolyte, with a scan rate of 10.0 mV s⁻¹ and a rotating speed of 1600 rpm.

electrocatalysis, facilitating the desorption of O_2 or H_2O , thus improving the OER and ORR reactivity.^[8,10] Recently, the anion modulation in oxygen electrode catalysts is attracting attention and has been demonstrated to be effective in improving the catalytic activity.^[10,20] In this contribution, the binding energy of Co 2p exhibits a downshift after sulfurization (Figure S10, Supporting Information), indicating a decrease in the Co oxidation state. A downshift of the binding energy is also observed in the XPS Co 2p spectra of CoAl-OH and $Co_5AlS_{1.5}(OH)_{10}$ (Figure S11, Supporting Information). Therefore, it is inferred that sulfurization can also effectively alter the electronic properties of Co, analogous to the cation modulation of Fe, thus leading to better catalytic activity. Moreover, compared with O atoms, S atoms can adjust the electronic structure of the adjacent Co atoms to be more dispersed, thus facilitating the interaction between Co and O-containing species in the oxygen electrocatalytic process. However, with a higher S content and a lower Co 2p binding energy, $CoFeS_{1.6}(OH)_{1.8}$ -HT affords inferior activity to $Co_3FeS_{1.5}(OH)_6$. This suggests that efficient oxygen catalysis requires a moderate Co oxidation state, and an oxidation state that is too low is unfavorable for the activity. This relationship between the state of the active site and the reactivity is exactly consistent with the tendency reflected by the volcano plot.

The OER and ORR performance of $Co_3FeS_{1.5}(OH)_6$ is also compared with CoFe-OH and Co-OH-S (synthesized in the same way as $Co_3FeS_{1.5}(OH)_6$, only without Fe doping) (Figure S12, Supporting Information). The E_{10} , $E_{1/2}$, and ΔE of these catalysts are listed in Table S3 (Supporting Information). The bifunctional activity of $Co_3FeS_{1.5}(OH)_6$ surpasses those of both the CoFe-OH and Co-OH-S catalysts, thus confirming the role of cation and anion modulation in the current CoFe hydroxysulfides. The bifunctional activities of the reported sulfide and cobalt-iron-based catalysts are also listed in Table S3 (Supporting Information). The low ΔE of $Co_3FeS_{1.5}(OH)_6$ elucidates the superiority of the transition metal hydroxysulfides through room-temperature sulfidization.

One major application for OER/ORR bifunctional catalysts is the Zn-air battery because Zn-air batteries are promising next-generation energy storage devices that possess high capacity and intrinsic safety advantages. The efficient transformation between oxygen and water on the air electrode is critical for high-performance Zn-air batteries.^[17,21] Demonstrated as an efficient bifunctional catalyst for OER and ORR, $Co_3FeS_{1.5}(OH)_6$ was utilized as the air electrode catalyst in a Zn-air battery. The precious metal catalysts Pt/C and Ir/C and their mixture (Pt/C + Ir/C, mass ratio 1:1) were also investigated in Zn-air batteries for comparison.

The Zn-air battery was fabricated using catalyst-coated carbon cloth as the air cathode, Zn foil as the anode, and 6.0 M KOH + 0.2 M $ZnCl_2$ as the electrolyte (see the illustration of Zn-air battery in Figure 4a). Figure 4b illustrates the polarization curves for the rechargeable Zn-air batteries. The potentials required for 20.0 mA cm^{-2} discharge and charge current densities on CoFe-S hydroxysulfides are 1.16 and 2.02 V, respectively. This performance surpasses Pt/C (0.90 and 2.54 V) and Ir/C (0.79 and 2.05 V) and is even better than the mixture of Pt/C and Ir/C (0.99 and 2.07 V). The maximum power density of $Co_3FeS_{1.5}(OH)_6$ is 113.1 mW cm^{-2} , outperforming all precious metal catalysts in this work.

The specific capacity was tested at a discharge current density of 20.0 mA cm^{-2} and was normalized to the mass of Zn (Figure 4c). The specific capacity of $Co_3FeS_{1.5}(OH)_6$ was measured to be 898 mAh g^{-1} , which is higher than that of the commercial Pt/C ORR catalyst (843 mAh g^{-1}). The charge-discharge properties of $Co_3FeS_{1.5}(OH)_6$ and Pt/C + Ir/C at a current density of 2.0 mA cm^{-2} are presented in Figure 4d, and $Co_3FeS_{1.5}(OH)_6$ showed a smaller charge-discharge voltage range, especially benefitting from the low charging voltage.

The cycling stability of $Co_3FeS_{1.5}(OH)_6$ hydroxysulfides as the air cathode of the Zn-air battery was also tested (Figure 4e). The charging/discharging current density is 2.0 mA cm^{-2} , with an initial discharging voltage of 1.14 V and an initial charging voltage of 1.98 V on $Co_3FeS_{1.5}(OH)_6$ hydroxysulfides. During the stability test, the CO_2 in the atmosphere can be adsorbed by the KOH electrolyte and can affect the long-term stability.^[22] Therefore, the electrolyte in the cell was replaced by fresh electrolyte every 4 h to eliminate the influence of CO_2 . After a 36 h test for 108 cycles, the discharging and charging voltages become 1.16 and 2.00 V, and the charge-discharge voltage gap maintains the initial value of 0.84 V. All of the above results verify the excellent activity and stability of the $Co_3FeS_{1.5}(OH)_6$ catalyst in ORR/OER catalysis and Zn-air batteries.

Some recent works have reported improved bifunctional OER/ORR catalysis on sulfide electrocatalysts. However, most of them are achieved through a high-temperature hydrothermal process in which the as-obtained sulfides have a large size of more than 20 nm.^[10,23] Therefore, the sulfide-based electrocatalysts either had limited exposed active sites or a lack of sophisticated spectroscopic evidence in the interactions between active sites and supports. Therefore, new insight into the interfacial mechanism is highly sought after to guide the advanced energy material design.^[7,24,25] From a molecular perspective, both hydrophilicity and high intrinsic reactivity are essential for oxygen electrocatalysis in aqueous electrolyte.^[26] On the one hand, a high affinity to H_2O allows the enrichment of feedstock at the surface, preventing the sluggish OH^- transfer from the fully solvated states. On the other hand, the anion regulated metal cations are expected to possess a high reactivity for oxygen conversion.^[27] The $Co_3FeS_{1.5}(OH)_6$ hydroxysulfide material reported herein thus has many elements that are conceptually novel, including (1) the rational integration of hydroxides and sulfides at an atomic scale to realize bifunctional electrocatalysis; (2) a fine-tuned strain confirmed by XRD and XPS to tune the adsorption of oxygen/water, indicating an emerging approach to regulate the OER/ORR electrochemistry; (3) the rational structural integration to obtain 3D intercrossed charge-transferring and ion-diffusion capabilities; (4) robust structural stability due to the well-preserved pomegranate-like nanostructure of the CoFe-OH to $Co_3FeS_{1.5}(OH)_6$ hydroxysulfides, which is a self-limited conversion in a confined space; and (5) the facile formation of advanced nonprecious metal hydroxysulfides from earth-abundant materials through a mild and green room-temperature sulfurization and their implementation as advanced electrocatalysts for Zn-air batteries, thus proposing a material-efficient route toward fully demonstrating the desirable merits from their components and related energy chemistry. However, for practical applications, the fading capacity of highly active material-loaded Zn-air batteries is still one of the

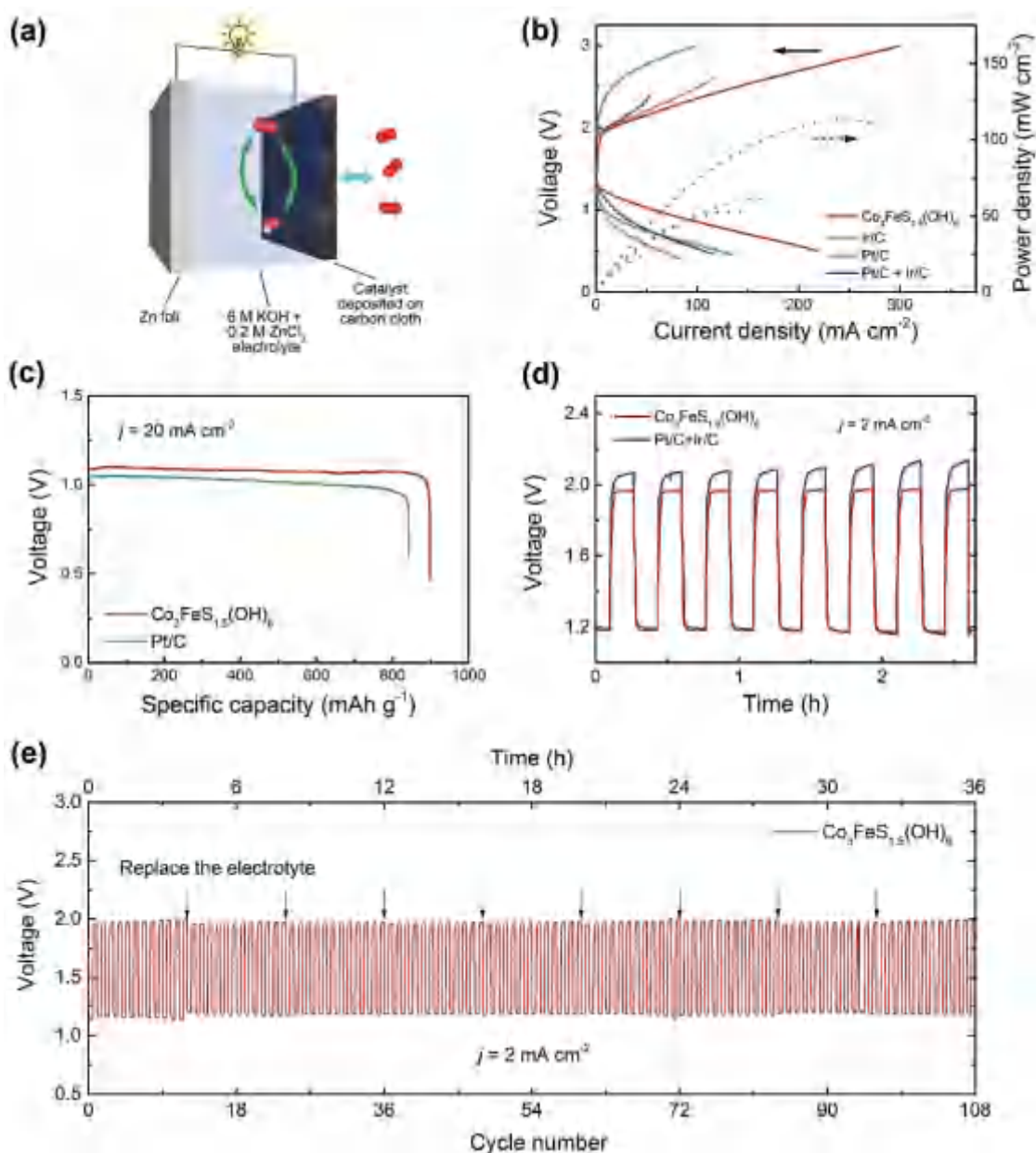


Figure 4. Zn–air battery tests on $\text{Co}_3\text{FeS}_{1.5}(\text{OH})_6$ and precious metal catalysts. a) The schematic diagram of Zn–air battery. b) Charge/discharge polarization and power density curves of $\text{Co}_3\text{FeS}_{1.5}(\text{OH})_6$, Ir/C, Pt/C, and Pt/C + Ir/C. c) Discharge curves of $\text{Co}_3\text{FeS}_{1.5}(\text{OH})_6$ and Pt/C at a constant current density of 20 mA cm^{-2} . d) Charge–discharge cycling curves of $\text{Co}_3\text{FeS}_{1.5}(\text{OH})_6$ and Pt/C + Ir/C at the current density of 2.0 mA cm^{-2} . e) Long-time cycling performance of Zn–air battery with $\text{Co}_3\text{FeS}_{1.5}(\text{OH})_6$ as the air electrode catalyst.

major obstacles. Apart from designing a superb electrocatalyst cathode in this work, emerging methodologies for stabilizing the electrolyte/electrode interfaces, especially at the Zn metal anode side, are urgently demanded.

In conclusion, novel metal hydroxysulfides are proposed as efficient bifunctional OER/ORR catalysts, and a facile room-temperature sulfurization strategy is employed to synthesize metal hydroxysulfides with good morphology replication. This concept of a green conversion method of hydroxides to hydroxysulfides was verified using both CoAl and CoFe systems. Attributed to the efficient sulfurization and the morphology-preservation

feature of this method, the as-obtained $\text{Co}_3\text{FeS}_{1.5}(\text{OH})_6$ hydroxysulfides render excellent bifunctional OER/ORR activity with a small potential gap between E_{10} and $E_{1/2}$ of 0.867 V , which outperforms the commercial precious metal Ir/C and Pt/C electrocatalysts. The $\text{Co}_3\text{FeS}_{1.5}(\text{OH})_6$ hydroxysulfides were also employed in the air electrode for a high-performance rechargeable Zn–air battery with a small overpotential of 0.86 V at 20.0 mA cm^{-2} discharge and charge current density, a high specific capacity of 898 mAh g^{-1} , and a long cycling life. This work provides a very simple but effective approach for metal hydroxysulfide fabrication with delicate structural regulation.

This is expected to open new doors to materials innovation on transition metal (hydro/oxy)sulfides and their applications in hetero/electrocatalysis, supercapacitors, rechargeable batteries, sensors, electronic/optical devices, and healthcare applications.

Supporting Information

Supporting Information is available from the Wiley Online Library or from the author.

Acknowledgements

This work was supported by National Key Research and Development Program (Nos. 2016YFA0202500 and 2016YFA0200102) and Natural Scientific Foundation of China (No. 21422604). The authors thank Zi-jing Xia, Shu-Yuan Zhang, Xiao-Yang Cui, and Ling Zhong for helpful discussion.

Conflict of Interest

The authors declare no conflict of interest.

Keywords

bifunctional air cathodes, CoFe hydroxysulfides, layered double hydroxides, oxygen evolution reaction, oxygen reduction reaction, Zn–air batteries

Received: April 25, 2017

Revised: May 19, 2017

Published online:

- [1] a) W. Chen, C. Xia, H. N. Alshareef, *ACS Nano* **2014**, *8*, 9531; b) S. J. Bao, C. M. Li, C. X. Guo, Y. Qiao, *J. Power Sources* **2008**, *180*, 676; c) L. F. Shen, L. Yu, H. B. Wu, X. Y. Yu, X. G. Zhang, X. W. Lou, *Nat. Commun.* **2015**, *6*, 6694; d) X. Y. Yu, L. Yu, X. W. Lou, *Adv. Energy Mater.* **2016**, *6*, 1501333; e) X. Xu, W. Liu, Y. Kim, J. Cho, *Nano Today* **2014**, *9*, 604.
- [2] C. H. Lai, M. Y. Lu, L. J. Chen, *J. Mater. Chem.* **2012**, *22*, 19.
- [3] a) F. Y. Cheng, J. Chen, *Chem. Soc. Rev.* **2012**, *41*, 2172; b) Y. Jiao, Y. Zheng, M. T. Jaroniec, S. Z. Qiao, *Chem. Soc. Rev.* **2015**, *44*, 2060; c) N.-T. Suen, S.-F. Hung, Q. Quan, N. Zhang, Y.-J. Xu, H. M. Chen, *Chem. Soc. Rev.* **2017**, *46*, 337.
- [4] a) H. Osgood, S. V. Devaguptapu, H. Xu, J. Cho, G. Wu, *Nano Today* **2016**, *11*, 601; b) M. Kuang, G. F. Zheng, *Small* **2016**, *12*, 5656.
- [5] a) Y. Gorlin, T. F. Jaramillo, *J. Am. Chem. Soc.* **2010**, *132*, 13612; b) F. Y. Cheng, J. A. Shen, B. Peng, Y. D. Pan, Z. L. Tao, J. Chen, *Nat. Chem.* **2011**, *3*, 79; c) K. L. Pickrahn, S. W. Park, Y. Gorlin, H. B. R. Lee, T. F. Jaramillo, S. F. Bent, *Adv. Energy Mater.* **2012**, *2*, 1269.
- [6] a) Q. Liu, J. T. Jin, J. Y. Zhang, *ACS Appl. Mater. Interfaces* **2013**, *5*, 5002; b) P. Ganesan, M. Prabhu, J. Sanetuntikul, S. Shanmugam, *ACS Catal.* **2015**, *5*, 3625; c) G. L. Tian, M. Q. Zhao, D. S. Yu, X. Y. Kong, J. Q. Huang, Q. Zhang, F. Wei, *Small* **2014**, *10*, 2251; d) P. Z. Chen, T. P. Zhou, L. L. Xing, K. Xu, Y. Tong, H. Xie, L. D. Zhang, W. S. Yan, W. S. Chu, C. Z. Wu, Y. Xie, *Angew. Chem., Int. Ed.* **2017**, *56*, 610; e) J. Yin, Y. X. Li, F. Lv, Q. H. Fan, Y. Q. Zhao, Q. L. Zhang, W. Wang, F. Y. Cheng, P. X. Xi, S. J. Guo, *ACS Nano* **2017**, *11*, 2275; f) J. Zhang, J. Fu, X. P. Song, G. P. Jiang, H. Zarrin, P. Xu, K. C. Li, A. P. Yu, Z. W. Chen, *Adv. Energy Mater.* **2016**, *6*, 1600476; g) Y. J. Ding, Y. C. Niu, J. Yang, L. Ma, J. G. Liu, Y. J. Xiong, H. X. Xu, *Small* **2016**, *12*, 5414; h) J. Qi, W. Zhang, R. J. Xiang, K. Q. Liu, H. Y. Wang, M. X. Chen, Y. Z. Han, R. Cao, *Adv. Sci.* **2015**, *2*, 1500199; i) W. J. Jiang, L. Gu, L. Li, Y. Zhang, X. Zhang, L. J. Zhang, J. Q. Wang, J. S. Hu, Z. D. Wei, L. J. Wan, *J. Am. Chem. Soc.* **2016**, *138*, 3570.
- [7] S. Dou, L. Tao, J. Huo, S. Y. Wang, L. M. Dai, *Energy Environ. Sci.* **2016**, *9*, 1320.
- [8] J. Yang, G. X. Zhu, Y. J. Liu, J. X. Xia, Z. Y. Ji, X. P. Shen, S. K. Wu, *Adv. Funct. Mater.* **2016**, *26*, 4712.
- [9] P. Cai, J. Huang, J. Chen, Z. Wen, *Angew. Chem., Int. Ed.* **2017**, *56*, 4858.
- [10] X. Han, C. Yu, S. Zhou, C. Zhao, H. Huang, J. Yang, Z. Liu, J. Zhao, J. Qiu, *Adv. Energy Mater.* **2017**, *7*, 1602148.
- [11] a) X. H. Xia, C. R. Zhu, J. S. Luo, Z. Y. Zeng, C. Guan, C. F. Ng, H. Zhang, H. J. Fan, *Small* **2014**, *10*, 766; b) B. Dong, X. Zhao, G. Q. Han, X. Li, X. Shang, Y. R. Liu, W. H. Hu, Y. M. Chai, H. Zhao, C. G. Liu, *J. Mater. Chem. A* **2016**, *4*, 13499.
- [12] W. Chen, H. T. Wang, Y. Z. Li, Y. Y. Liu, J. Sun, S. H. Lee, J. S. Lee, Y. Cui, *ACS Cent. Sci.* **2015**, *1*, 244.
- [13] L. Zhou, M. Shao, C. Zhang, J. Zhao, S. He, D. Rao, M. Wei, D. G. Evans, X. Duan, *Adv. Mater.* **2017**, *29*, 1604080.
- [14] a) A. M. Wiltrout, C. G. Read, E. M. Spencer, R. E. Schaak, *Inorg. Chem.* **2016**, *55*, 221; b) Z. Peng, D. S. Jia, A. M. Al-Enizi, A. A. Elzatahry, G. F. Zheng, *Adv. Energy Mater.* **2015**, *5*, 1402031.
- [15] J. H. Wang, W. Cui, Q. Liu, Z. C. Xing, A. M. Asiri, X. P. Sun, *Adv. Mater.* **2016**, *28*, 215.
- [16] a) H. F. Wang, C. Tang, X. L. Zhu, Q. Zhang, *J. Mater. Chem. A* **2016**, *4*, 3379; b) M. S. Burke, M. G. Kast, L. Trotochaud, A. M. Smith, S. W. Boettcher, *J. Am. Chem. Soc.* **2015**, *137*, 3638; c) X. L. Zhu, C. Tang, H. F. Wang, B. Q. Li, Q. Zhang, C. Y. Li, C. H. Yang, F. Wei, *J. Mater. Chem. A* **2016**, *4*, 7245; d) B. Q. Li, C. Tang, H. F. Wang, X. L. Zhu, Q. Zhang, *Sci. Adv.* **2016**, *2*, e1600495.
- [17] X. Liu, M. Park, M. G. Kim, S. Gupta, G. Wu, J. Cho, *Angew. Chem., Int. Ed.* **2015**, *54*, 9654.
- [18] N. Kornienko, J. Resasco, N. Becknell, C. M. Jian, Y. S. Liu, K. Q. Nie, X. H. Sun, J. H. Guo, S. R. Leone, P. D. Yang, *J. Am. Chem. Soc.* **2015**, *137*, 7448.
- [19] a) A. Indra, P. W. Menezes, N. R. Sahaie, A. Bergmann, C. Das, M. Tallarida, D. Schmeisser, P. Strasser, M. Driess, *J. Am. Chem. Soc.* **2014**, *136*, 17530; b) Y. Yang, H. L. Fei, G. D. Ruan, C. S. Xiang, J. M. Tour, *ACS Nano* **2014**, *8*, 9518.
- [20] J. J. Duan, S. Chen, A. Vasileff, S. Z. Qiao, *ACS Nano* **2016**, *10*, 8738.
- [21] a) J. T. Zhang, Z. H. Zhao, Z. H. Xia, L. M. Dai, *Nat. Nanotechnol.* **2015**, *10*, 444; b) Y. G. Li, M. Gong, Y. Liang, J. Feng, J. E. Kim, H. L. Wang, G. S. Hong, B. Zhang, H. J. Dai, *Nat. Commun.* **2013**, *4*, 1805; c) J. Fu, Z. P. Cano, M. G. Park, A. P. Yu, M. Fowler, Z. W. Chen, *Adv. Mater.* **2017**, *29*, 1604685; d) C. Tang, H. F. Wang, X. Chen, B. Q. Li, T. Z. Hou, B. S. Zhang, Q. Zhang, M. M. Titirici, F. Wei, *Adv. Mater.* **2016**, *28*, 6845; e) S. Chen, J. J. Duan, Y. Zheng, X. M. Chen, X. W. Du, M. Jaroniec, S. Z. Qiao, *Energy Storage Mater.* **2015**, *1*, 17; f) Y. L. Liu, F. J. Chen, W. Ye, M. Zeng, N. Han, F. P. Zhao, X. X. Wang, Y. G. Li, *Adv. Funct. Mater.* **2017**, *27*, 1606034; g) Y. G. Li, H. J. Dai, *Chem. Soc. Rev.* **2014**, *43*, 5257; h) M. G. Park, D. U. Lee, M. H. Seo, Z. P. Cano, Z. W. Chen, *Small* **2016**, *12*, 2707.
- [22] H. B. Yang, J. W. Miao, S. F. Hung, J. Z. Chen, H. B. Tao, X. Z. Wang, L. P. Zhang, R. Chen, J. J. Gao, H. M. Chen, L. M. Dai, B. Liu, *Sci. Adv.* **2016**, *2*, e1501122.
- [23] S. Huang, Y. Meng, S. He, A. Goswami, Q. Wu, J. Li, S. Tong, T. Asefa, M. Wu, *Adv. Funct. Mater.* **2017**, *27*, 1606585.
- [24] C. Tang, H. F. Wang, X. L. Zhu, B. Q. Li, Q. Zhang, *Part. Part. Syst. Charact.* **2016**, *33*, 473.

- [25] a) W. J. Lee, J. Lim, S. O. Kim, *Small Methods* **2017**, *1*, 1600014; b) X. L. Zhao, F. Li, R. N. Wang, J. M. Seo, H. J. Choi, S. M. Jung, J. Mahmood, I. Y. Jeon, J. B. Baek, *Adv. Funct. Mater.* **2017**, *27*, 1605717; c) X. M. Xu, C. Su, W. Zhou, Y. L. Zhu, Y. B. Chen, Z. P. Shao, *Adv. Sci.* **2016**, *3*, 1500187.
- [26] a) C. Tang, Q. Zhang, *Adv. Mater.* **2017**, *29*, 1604103; b) G. L. Tian, Q. Zhang, B. S. Zhang, Y. G. Jin, J. Q. Huang, D. S. Su, F. Wei, *Adv. Funct. Mater.* **2014**, *24*, 5956; c) J. T. Zhang, H. L. Li, P. Z. Guo, H. Y. Ma, X. S. Zhao, *J. Mater. Chem. A* **2016**, *4*, 8497; d) S. Gupta, L. Qiao, S. Zhao, H. Xu, Y. Lin, S. V. Devaguptapu, X. L. Wang, M. T. Swihart, G. Wu, *Adv. Energy Mater.* **2016**, *6*, 1601198.
- [27] a) J. F. Zhang, Y. C. Hu, D. L. Liu, Y. Yu, B. Zhang, *Adv. Sci.* **2017**, *4*, 1600343; b) B. Q. Li, S. Y. Zhang, C. Tang, Q. Zhang, *Small* **2017**, *13*, 1700610; c) X. Long, G. X. Li, Z. L. Wang, H. Y. Zhu, T. Zhang, S. Xiao, W. Y. Guo, S. H. Yang, *J. Am. Chem. Soc.* **2015**, *137*, 11900.